ChemPubSoc Europe

DOI: 10.1002/chem.201804360

CHEMISTRY A European Journal Full Paper

Nanomaterials

Solution-Processable Two-Dimensional In_2Se_3 Nanosheets as Efficient Photothermal Agents for Elimination of Bacteria

Chunli Zhu[+], Haijing Shen[+], Haoyang Liu, Xiaobo Lv, Zhihao Li, and Quan Yuan*[a]

Abstract: Two-dimensional (2D) nanoflakes represent an appealing class of materials for optoelectronics applications due to their unique layered structures and excellent electronic properties. However, the lack of easy-to-manipulate and effective methods for large-scale production of these 2D materials limits their potential for applications. Also, few efforts have been made to explore their applications in biological fields. This work reports the preparation of large quantities of 2D In_2Se_3 nanosheets through a solvent exfoliation technique. Transmission electron microscopy and atomic force microscopy results show that the In_2Se_3 nanosheets are obtained with lateral sizes of tens of nanometers to hundreds of nanometers and thickness of 2–17 layers. Raman features coupled with the X-ray diffractometry results unequivocally confirm the as-prepared In_2Se_3 nanosheets to be α phase. Moreover, these α-In_2Se_3 nanosheets exhibit an excellent near-infrared (NIR) photothermal performance under an 808 nm laser irradiation. NIR photo-excitation of the α-In_2Se_3 nanosheets in the presence of bacteria leads to a significant antibacterial effect, suggesting that these nanosheets have great potential to be photothermal antibacterial agents. Our work on α-In_2Se_3 nanosheets presents an available method for exfoliating 2D layered materials, and highlights the potential application in chemical and biological fields of α-In_2Se_3 nanosheets.

Introduction

Two-dimensional (2D) materials with sheet-liked structures have attracted tremendous attention in optoelectronics, electronics, and biomedicine (e.g., therapy, imaging/diagnosis, and biosensors) in recent years.[1–9] So far, a large number of 2D crystals have been explored, including black phosphorus (BP), transition metal dichalcogenides (TMDCs), and transition metal oxides (TMOs).[10–14] Thanks to the weak van der Waals forces between layers, the parent layered bulk materials can be split into thin sheets with several layers.[15,16] These layered crystals exhibit appealing physical and chemical characteristics such as semiconducting behavior, nonlinear optics, and valleytronics as well. Furthermore, scientists indicate that these crystals behaviors rely heavily on the thickness of obtained nanosheets.[17] Indium (III) selenide (In_2Se_3) represents a typical class of layered $A_2^{III}B_3^{VI}$ compound semiconductor, consisting of [Se-In-Se-In-Se] layers held together through the van der Waals interactions.[18] Like other layered 2D materials, it is likely that In_2Se_3 nanosheets are of great interest for a wide range of applications from optoelectronics to photovoltaic devices,[19] and so on. Most recently, tremendous efforts have been made for the preparation of In_2Se_3 nanosheets, including chemical vapor deposition (CVD), physical vapor deposition (PVD), and micromechanical exfoliation.[17,20,21] However, micromechanical exfoliation cannot carry out the large-scale production, and CVD/PVD processes need stringent conditions such as high temperature and specific airflow velocity. Additionally, the studies of In_2Se_3 mainly focus on its physical properties, while no efforts have been made to explore its application in other areas, such as chemical or biological fields. As a consequence, it is of great significance to develop a robust and available method to produce large quantities of In_2Se_3 nanosheets, and further expand their biochemical applications.

Liquid-phase exfoliation has recently received considerable attention in the production of 2D nanomaterials.[22,23] This method allows the delamination of bulk layered crystals to 2D thin nanosheets by exposure to ultrasonication in liquid. The physical basis for exfoliation is based on an energy match between the surface of the 2D crystals and the solvent.[24] These layered materials can strongly adsorb solvent molecules into the spacing between adjacent layers. Then, the intercalation of guest molecules can expand the interlayer spacing, weakening the interlayer van der Waals bonding and further peeling off thin 2D nanosheets.[25] The lateral size and thickness of the resultant 2D nanosheets can be controlled by judiciously tuning the exfoliation conditions, such as ultrasonic frequency, time, and solvent type. Moreover, size-selected nanosheets can be achieved by controlled centrifugation, enabling dispersing in liquids stably for further use. Additionally, the solvent exfolia-

[a] C. Zhu,[+] H. Shen,[+] H. Liu, X. Lv, Z. Li, Prof. Q. Yuan
Key Laboratory of Analytical Chemistry for Biology and Medicine (Ministry of Education)
College of Chemistry and Molecular Sciences
Wuhan University, Wuhan 430072 (P.R. China)
E-mail: yuanquan@whu.edu.cn

[+] These authors contributed equally to this work.

Supporting information and the ORCID identification number(s) for the author(s) of this article can be found under: https://doi.org/10.1002/chem.201804360.

tion technique is low-cost, simple to implement, and potentially appropriate for the large-scale production. Thus, solvent exfoliation technique is a promising approach for mass production of solution-processable 2D nanosheets with desired physical and chemical properties, and could have a transformative effect on materials science and technology.

Due to the excellent photothermal properties in the near-infrared (NIR) region, NIR photothermal agents have generated broad interest in antibacterial treatment, drug delivery, tissue engineering, and cancer photothermal therapy.[26–28] Although various 2D materials such as graphene,[5] molybdenum disulfide,[29] and black phosphorus (BP),[23] have been used as effective photothermal agents, the exploitation of new types of photothermal agents is of great scientific and clinical interest. So far, the photothermal properties of In_2Se_3 nanosheets have not been explored. In this regard, the investigation of the photothermal properties of In_2Se_3 can help to exploit the potential of biochemical application of In_2Se_3 nanosheets. Herein, we develop a solvent exfoliation technique for the production of solution-processable 2D In_2Se_3 nanosheets. Importantly, for the first time, we highlight that the In_2Se_3 nanosheets exhibit good photothermal properties with excellent photothermal conversion efficiency under NIR laser irradiation. The In_2Se_3 nanosheets coupled with NIR irradiation are applied as antibacterial agents. The photothermal character of In_2Se_3 nanosheets indicates that they can be highlighted as an emerging and ideal photothermal platform for antibacterial therapy and cancer therapy.

Results and Discussion

As shown in Scheme 1, bulk In_2Se_3 is exfoliated by a solvent exfoliation technique that involves ultrasound probe sonication in N-methyl-2-pyrrolidone (NMP) solution. The In_2Se_3 nanosheets were obtained by controlled centrifugation. Transmission electron microscopy (TEM) was used to investigate the

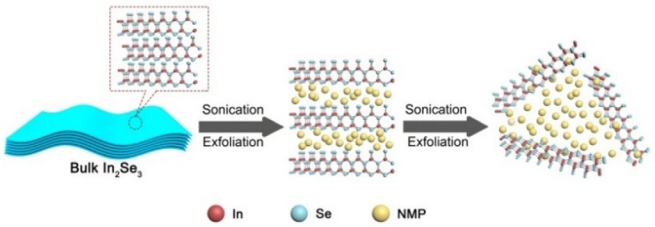

Scheme 1. Schematic illustration of the preparation of In_2Se_3 nanosheets.

morphology of the obtained In_2Se_3 nanosheets. As shown in Figure 1 a, the individual and scattered In_2Se_3 nanosheets with amorphous morphology are observed, and their lateral sizes are measured to be of about 300 nm. The inset image in Figure 1 a depicts the photograph of the NMP solution containing exfoliated In_2Se_3 nanosheets. The brown color of the suspension is observed, and these solution-processable In_2Se_3 nanosheets exhibit excellent stability and dispersibility in NMP, indi-

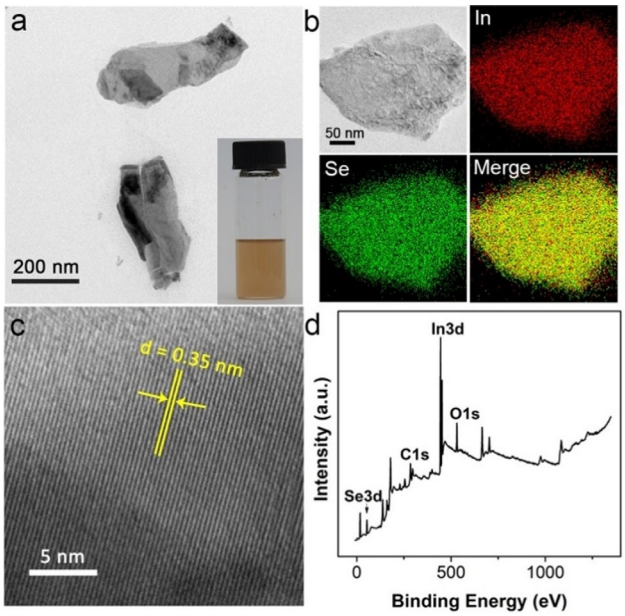

Figure 1. (a) TEM image of In_2Se_3 nanosheets. Inset: Photograph of In_2Se_3 nanosheets dispersed in NMP solution. (b) TEM image (at higher magnification) and elemental mapping images of the In_2Se_3 nanosheets. (c) HRTEM image of the In_2Se_3 nanosheets. (d) Full scale XPS scan of In_2Se_3 nanosheets.

cating the efficient exfoliation of In_2Se_3. The elemental mapping in Figure 1 b shows that both In and Se are homogeneously distributed across the flake. Atomic force microscopy (AFM) image shows that these In_2Se_3 flakes appear with heights from 2 to 17 nm, indicating that obtained In_2Se_3 nanosheets were about 2–17 layers. (Figure S1, Supporting Information).[20] In bulk or thin-flake In_2Se_3, the properties such as band gap, and sensitivity largely depend on stoichiometry and phase, resulting in inconsistent performances.[30] Recent researches suggest that In_2Se_3 exists in five crystalline forms (α, β, γ, δ, and κ).[31,32] Among them, α-phase and β-phase are the two common forms sharing a layered crystalline structure.[11] X-ray diffractometry (XRD) was conducted to determine the crystallographic phase of the as-prepared In_2Se_3 nanosheets. The peaks shown in XRD data exhibit primarily the characteristic of α-phase (Figure S4).[33] Furthermore, the high-resolution TEM (HRTEM) image in Figure 1 c reveals highly crystallinity of the nanosheets with a lattice spacing of about 0.35 nm, consistent with the (1–100) plane of the hexagonal α-In_2Se_3.[30] X-ray photoelectron spectroscopy (XPS) was also conducted to analyze the composition of the obtained nanosheets. It is clear that only In and Se elements can be found in the full scale spectrum, whereas C and O are in accordance with the reference (Figure 1 d). High resolution XPS spectra of In 3d and Se 3d are shown in Figure S5. Peaks located at 444.2 eV and 451.8 eV originated from the In $3d_{5/2}$ and In $3d_{3/2}$ doublets, respectively. The peaks appearing at 53.9 eV and 59.1 eV originated from the Se $3d_{5/2}$ and Se $3d_{3/2}$ binding energies. These spectral features all confirm a pure phase of In_2Se_3.[34]

Spectroscopic technologies containing Raman spectrum and photoluminescence (PL) were further applied to investigate the quality and property of the as-prepared In_2Se_3 nanosheets.

The Raman spectra shown in Figure 2a were collected with a 532 nm laser as the light source. Three Raman peaks at ≈102, ≈180, and ≈196 cm^{-1} are observed in both bulk In_2Se_3 and In_2Se_3 nanosheets, which originated from A_1 (LO + TO), A_1 (TO), and A_1 (LO) modes, respectively.[20,35] Moreover, there is nearly no difference between bulk In_2Se_3 and In_2Se_3 nanosheets, indicating that sonication causes negligible damage to the structure of In_2Se_3. The Raman features coupled with the XRD result unambiguous identify the exfoliated In_2Se_3 nanosheets to be α phase. The PL properties of bulk In_2Se_3 and In_2Se_3 nanosheets were obtained at room temperature, as shown in Figure 2b. The bulk In_2Se_3 exhibits a weak PL signal, but a strong PL signal located at 830 nm is found in exfoliated In_2Se_3 nanosheets. Supposedly, this PL property may contribute to the synergistic effects of the carrier confinement across the *xy*-plane as well as along the *z*-axis.[36] The PL property of In_2Se_3 nanosheets makes it an emerging NIR imaging material.

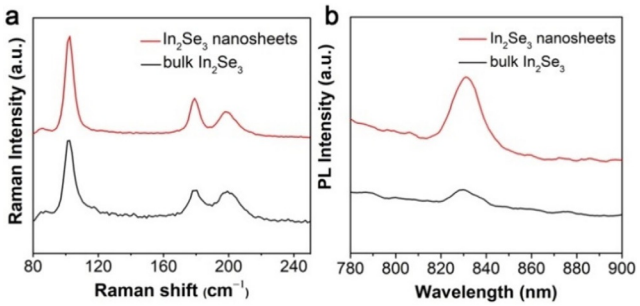

Figure 2. (a) Raman spectra and (b) PL spectra of the In_2Se_3 nanosheets and bulk In_2Se_3.

The NIR extinction of In_2Se_3 nanosheets suspension was characterized by the optical absorption spectra. As shown in Figure 3a, the acquired absorption spectra show a broad absorption band spanning the UV/Vis-NIR regions and the absorption intensity gradually decreases along with the reduction of concentration of In_2Se_3 nanosheets suspension. This character of the optical absorption spectra is similar to that of other 2D layered materials, such as BP[27] and graphene oxide (GO).[37,38] The normalized absorption intensity of In_2Se_3 nanosheets at 808 nm over length of the cell (A/L) was monitored at different concentrations (C). As shown in Figure 3b, A/L at 808 nm showed a linear trend on the concentration, which is consistent with the Lambert–Beer law ($A/L = \alpha C$, where α represents the extinction coefficient). The extinction coefficient of In_2Se_3 nanosheets at 808 nm is estimated to be 2.4 $L\,g^{-1}\,cm^{-1}$, which is slightly under that of GO nanosheets.[19] These results above indicate that In_2Se_3 nanosheets are potential photothermal agents. To investigate the photothermal performance of the In_2Se_3 nanosheets, different concentrations of In_2Se_3 nanosheet suspensions were irradiated with an 808 nm NIR laser. The temperature of the suspension was then monitored over time (Figure 3c). After irradiating with an 808 nm laser for 15 min, the final temperature elevation gradually increases with the increasing concentration of In_2Se_3 nanosheets. At a certain concentration (150 ppm), the temperature of the In_2Se_3 suspension increases to 53 °C, while the temperature of pure water only increases to 31 °C. These photothermal results indicate that the In_2Se_3 nanosheets have excellent photothermal conversion efficiency under NIR laser irradiation. Furthermore, to investigate the photothermal stability of In_2Se_3 nanosheets, In_2Se_3 nanosheets suspension was irradiated with NIR laser, followed by natural cooling to room temperature after turning down the laser. This same cycle was repeated six times and the temperature was monitored with time. As shown in Figure 3d, the photothermal performance remains good during temperature elevation and photothermal cycle, highlighting that the In_2Se_3 nanosheets can be applied as a potential photothermal agent.

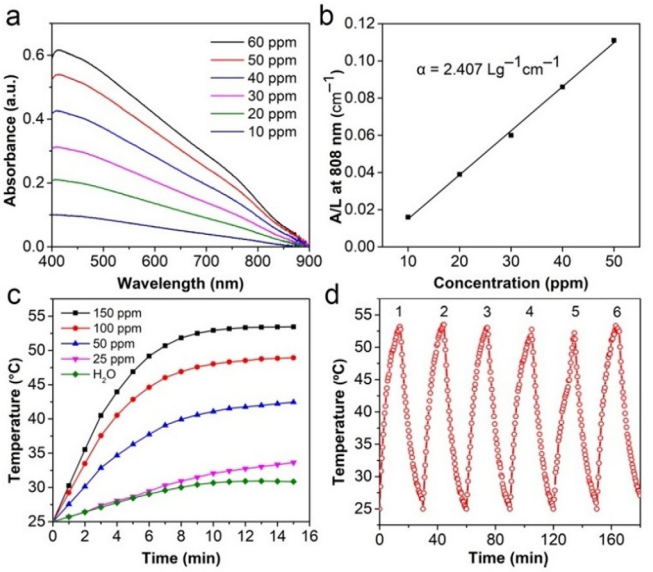

Figure 3. (a) Absorbance spectra of In_2Se_3 nanosheet suspensions at different concentrations. (b) Normalized absorbance intensity at 808 nm over the characteristic length of the cell (A/L) at different concentrations. (c) Photothermal heating curves of water and In_2Se_3 nanosheets suspensions at different concentrations under 808 nm irradiation (3.0 $W\,cm^{-2}$). (d) Photothermal cycle curve of the In_2Se_3 nanosheets suspensions with six laser on/off cycles.

The photothermal effect of In_2Se_3 nanosheets for anti-microbial applications was next investigated, as shown in Figure 4. When *E. coli* cells were only incubated with the In_2Se_3 nanosheets (In_2Se_3 concentration is 0, 50, 100, and 150 ppm) for 2 hours, there are still plenty of bacteria alive even at the relative high concentration of 150 ppm (Figure 4a, top). In contrast, when the bacteria were incubated with various concentrations of In_2Se_3 nanosheets and then exposed to the 808 nm laser for 10 min, a dose-dependent antibacterial effect can be observed. The bacterial viabilities are apparently reduced with the increasing concentrations of In_2Se_3 nanosheets (Figure 4a, down). Clearly, at the relative low concentration of In_2Se_3 nanosheets (150 ppm), almost all of the bacteria are killed under NIR irradiation, and the bacterial inactivation percentage is 98% (Figure 4b). Moreover, Gram-positive bacteria (*S. aureus*) can also be eliminated effectively by the photothermal effect of In_2Se_3 nanosheets (Figure S10). Additionally, a fluorescent live/dead assay was carried out to visualize the antibacterial ability of In_2Se_3 nanosheets with NIR irradiation. Two fluores-

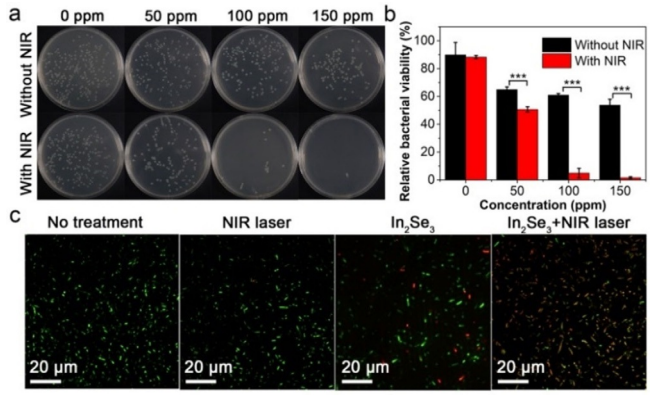

Figure 4. (a) Photographs of formed bacterial colonies of *E. coli* cells after being exposed to 0, 50, 100, and 150 ppm In_2Se_3 nanosheets without or with the NIR laser irradiation. (b) Relative bacterial viabilities of *E. coli* cells after incubation with 0, 50, 100, and 150 ppm In_2Se_3 nanosheets without or with 808 nm irradiation, determined by plate count method. $^{***}p < 0.001$ (the groups with NIR irradiation versus the groups without NIR irradiation), showing significant difference between the two groups. (c) Fluorescence images of bacteria stained with SYTO9 and PI.

cent dyes of SYTO9 and propidium iodide (PI) were used to discriminate live (green fluorescence) and dead (orange-red fluorescence) bacteria, respectively. As shown in Figure 4c, when bacteria are incubated with In_2Se_3 nanosheets, no significant cytotoxicity can be observed without NIR irradiation. However, when the bacteria were incubated with In_2Se_3 nanosheets and then exposed to the 808 nm laser, almost all of the bacteria were killed. These results show that bacteria can be effectively killed by the heat produced by In_2Se_3 nanosheets, confirming the suitability of In_2Se_3 nanosheets as an efficient photothermal agent.

As a real application, we also investigated the antibacterial activity of these obtained In_2Se_3 nanosheets in natural freshwater (East Lake, Wuhan, China). The water was first filtered through the filter membrane with a diameter of 0.22 μm and then spiked with bacteria for further use. The bacteria-contaminated water without treatment served as a control. As shown in Figure 5, no obvious bacterial inactivation is observed from

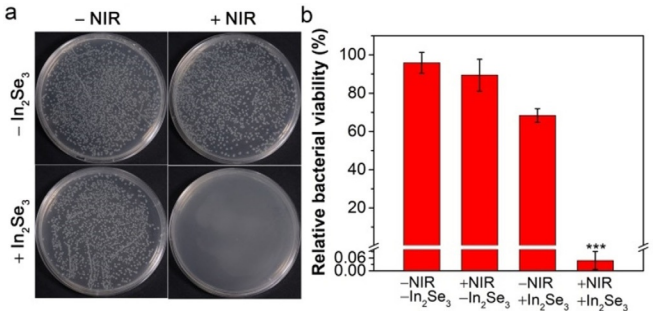

Figure 5. (a) Photographs of formed bacterial colonies of *E. coli* contaminated natural water after being exposed to 0 and 150 ppm In_2Se_3 nanosheets without or with the NIR laser irradiation. (b) Relative bacterial viabilities of *E. coli* cells after incubation with 0 and 150 ppm In_2Se_3 nanosheets without or with 808 nm irradiation, determined by plate count method. $^{***}p < 0.001$ (the groups with different treatment versus the control group), showing significant difference from the control group.

the water only exposed to NIR laser or incubated with the In_2Se_3 nanosheets, suggesting that the NIR light and the In_2Se_3 nanosheets do not have any significant antibacterial effect. Conversely, the water containing In_2Se_3 nanosheets shows a bacterial inactivation percentage of 99.99% under NIR irradiation. These results suggest that the hyperthermia produced by In_2Se_3 nanosheets with NIR irradiation has remarkable antibacterial effect in natural water system. Furthermore, the In_2Se_3 nanosheets can be easily separated by centrifugation or natural deposition, making it suitable for sterilization in natural water.

To further investigate the antibacterial behavior of the photothermal effect triggered by In_2Se_3 nanosheets, the morphology of bacteria were observed with scanning electron microscopy (SEM). As shown in Figure 6a,b, natural *E. coli* cells are rod-shaped with a smooth surface and integrated structure.

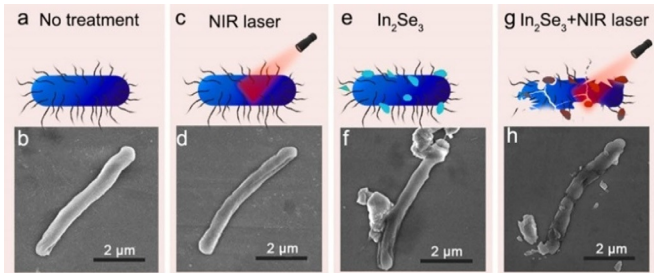

Figure 6. The illustrations (top) and corresponding SEM images (bottom) of *E. coli* cells under different conditions: (a,b) without treatment; (c,d) irradiated with 808 nm laser (3 W cm^{-2}); (e,f) incubated with In_2Se_3 (150 ppm); (g,h) incubated with In_2Se_3 (150 ppm) and irradiated with 808 nm laser (3 W cm^{-2}).

When the *E. coli* cells were only irradiated with NIR laser or incubated with the In_2Se_3 nanosheets, no obvious disruption on the cell walls is observed (Figure 6c–f), indicating NIR irradiation or In_2Se_3 nanosheets has no influence on the anti-microbial effects. In contrast, after irradiation with the NIR laser, the In_2Se_3 nanosheets-treated *E. coli* cells lose their integrity and the cell walls become partially wrinkled and cracked (Figure 6g,h). Notably, the group of In_2Se_3 nanosheets coupled with the NIR irradiation show much more violent damage on the bacterial integrity, indicating that the strong antibacterial ability is caused by the photothermal performance of In_2Se_3 nanosheets. In this case, it is speculate that the hyperthermia have greatly destructive effect on bacterial viability.[39] These results demonstrate that the In_2Se_3 nanosheets can be an efficient photothermal agent for anti-microbial applications.

Conclusions

In this work, we developed a solvent exfoliation technique for large-scale production of 2D α-In_2Se_3 nanosheets. The morphologies and sizes of the as-prepared nanosheets were confirmed by TEM and AFM characterization, showing that the In_2Se_3 nanosheets have lateral sizes of tens of nanometers to hundreds of nanometers and thicknesses of 2–17 layers. These

obtained In_2Se_3 nanosheets were characterized to be α phase by XRD and Raman measurements. Furthermore, the obtained α-In_2Se_3 nanosheets exhibit good photothermal performance under the NIR laser irradiation. The antibacterial results demonstrate that these α-In_2Se_3 nanosheets have excellent antibacterial capabilities owing to their photothermal properties. The liquid exfoliation technique we reported here will broaden the fabrication method of the whole family of 2D layered materials. Moreover, the photothermal performance of α-In_2Se_3 nanosheets can exploit their potential application in chemical and biological fields.

Experimental Section

Chemicals

The bulk In_2Se_3 with 150 μm diameter was purchased from Nanjing XFNANO Materials Tech Co., Ltd (Nanjing, China). The N-methyl-2-pyrrolidone (NMP), glutaraldehyde and ethanol were provided by Sinopharm Chemical Reagent Co., Ltd., China. Propidium Iodide (PI) (Solarbio, China), SYTO9 (Invitrogen, Carlsbad, CA), Bacto peptone (Becton, Dickenson & Co.), Yeast extract (Oxoid Ltd., Basingstoke, Hampshire, England.), agar (Vetec) and NaCl (Aladdin) were used without further purification.

Preparation of In_2Se_3 nanosheets

The In_2Se_3 nanosheets were prepared according to a liquid exfoliation technique.[40] Specifically, 500 mg of commercial bulk In_2Se_3 powders were dispersed in 300 mL of NMP. The mixture solution was sonicated in an ice bath with a sonic tip (ultrasonic frequency: 19–25 kHz) for 24 h (period of 6 s with the interval of 2 s) under argon protection. The obtained brown dispersion was centrifuged for 5 min at 4000 rpm to remove the massive particles. Then, the supernatant containing the In_2Se_3 nanosheets was centrifuged for 10 min at 6000 rpm. After drying in a vacuum drying oven for 4 h, the In_2Se_3 nanosheets were obtained.

NIR laser-induced heat conversion

In_2Se_3 nanosheets were dispersed in ultrapure water with final nanosheet concentrations of 25 ppm, 50 ppm, 100 ppm, and 150 ppm. The solutions were irradiated for 15 min using an 808 nm diode laser system (BWT Beijing Ltd, Beijing, China) with a power density of 3 W cm^{-2}. The ultrapure water and bulk In_2Se_3 were used as controls. The temperature was monitored by the FLIR A35 infrared thermal imaging camera (USA).

Antibacterial activity of In_2Se_3 nanosheets after NIR exposure

The *Escherichia coli* (*E. coli*) and *Staphylococcus aureus* (*S. aureus*) were used as model bacteria to examine the photothermal antibacterial activities of the In_2Se_3 nanosheets. Luria–Bertani (LB) broth medium consists of 10 g Bacto peptone, 5 g yeast extract, 15 g agar, and 10 g NaCl per liter of ultrapure water. Optical density (OD) at 600 nm was measured to confirm the concentration of bacteria. First, the bacterial suspensions with a certain concentration of 1.0×10^6 CFU per mL were mixed with In_2Se_3 nanosheets at different concentrations. After that, the suspensions were exposed to an 808 nm laser (3 W cm^{-2}) for 10 min and further incubated at 37 °C with shaking for 2 h. Then, 10 μL of suspension was spread on the LB medium and incubated at 37 °C. Colonies formed after incubation for 24 h. The relative bacterial viabilities were calculated based on colony counting method.[41] The relative bacterial viability of the untreated bacterial suspension was regarded as 100 %.

Antibacterial activity of In_2Se_3 nanosheets in natural water

The water was sampled from the west side of the East Lake (Wuhan, China) and then filtered through the filter membrane with a diameter of 0.22 μm. A certain concentration of bacteria (1.0×10^6 CFU per mL) was spiked into water for the following experiments. Four typical groups of the bacteria-contaminated water (a) without treatment, (b) exposed to 808 nm laser (3 W cm^{-2}), (c) incubated with In_2Se_3 (150 ppm), (d) incubated with In_2Se_3 (150 ppm) and exposed to 808 nm laser (3 W cm^{-2}) were incubated at 37 °C with shaking for 2 h. Then, 10 μL of suspension was spread on the LB medium and incubated at 37 °C. Colonies formed after incubation for 24 h. The relative bacterial viabilities were calculated based on colony counting method.[41] The relative bacterial viability of the untreated bacterial suspension was regarded as 100 %.

Morphology observation of *E. coli* cells

Four typical groups of the bacterial suspensions (1.0×10^9 CFU per mL) (a) without treatment, (b) irradiated with 808 nm laser (3 W cm^{-2}), (c) incubated with In_2Se_3 (150 ppm), (d) incubated with In_2Se_3 (150 ppm) and irradiated with 808 nm laser (3 W cm^{-2}) were fixed with 2.5 % glutaraldehyde overnight at 4 °C and then washed with PBS twice. 10 μL of the suspensions were dropped on silicon wafers and dried under room temperature. Then the dried bacteria cells were sputter-coated with Au for SEM image after being dehydrated by 25, 50, 75, and 100 % of ethanol, respectively for 15 min.

The live/dead bacterial assay

Four typical groups of the bacterial suspensions (1.0×10^9 CFU per mL) (a) without treatment, (b) irradiated with 808 nm laser (3 W cm^{-2}), (c) In_2Se_3 nanosheets (150 ppm), (d) In_2Se_3 nanosheets (150 ppm) and irradiated with 808 nm laser (3 W cm^{-2}) were stained with a fluorescent probe that contained 5 μM green-fluorescing SYTO9 and 15 μM red-fluorescing PI. After being incubated in the dark for 30 min, the bacteria were visualized on a PerkinElmer UltraVIEW VoX microscope with a ×60 objective lens.

Acknowledgements

This work was supported by the National Natural Science Foundation of China (21675120), National Key R&D Program of China (2017YFA0208000, 2016YFF0100800), National Basic Research Program of China (973 Program, Grants 2015CB932600) and Ten Thousand Talents Program for Young Talents. Q.Y. thanks the large-scale instrument and equipment sharing foundation of Wuhan University.

Conflict of interest

The authors declare no conflict of interest.

Keywords: anti-bacterial · In_2Se_3 · photothermal materials · solvent exfoliation · two-dimensional materials

[1] K. S. Novoselov, D. Jiang, F. Schedin, T. J. Booth, V. V. Khotkevich, S. V. Morozov, A. K. Geim, *Proc. Natl. Acad. Sci. USA* **2005**, *102*, 10451 – 10453.
[2] X. Wang, F. Xia, *Nat. Mater.* **2015**, *14*, 264 – 265.
[3] K. S. Novoselov, A. Mishchenko, A. Carvalho, A. H. C. Neto, *Science* **2016**, *353*, aac9439.
[4] X. Hu, Y. Wang, Y. Tan, J. Wang, H. Liu, Y. Wang, S. Yang, M. Shi, S. Zhao, Y. Zhang, Q. Yuan, *Adv. Mater.* **2017**, *29*, 1605235.
[5] K. Yang, S. Zhang, G. Zhang, X. Sun, S. T. Lee, Z. Liu, *Nano Lett.* **2010**, *10*, 3318 – 3323.
[6] X. Zhang, Y. Du, *RSC Adv.* **2016**, *6*, 17504 – 17509.
[7] C. Tan, X. Cao, X. J. Wu, Q. He, J. Yang, X. Zhang, J. Chen, W. Zhao, S. Han, G. H. Nam, M. Sindoro, H. Zhang, *Chem. Rev.* **2017**, *117*, 6225 – 6331.
[8] C. H. Lu, H. H. Yang, C. L. Zhu, X. Chen, G. N. Chen, *Angew. Chem. Int. Ed.* **2009**, *48*, 4785 – 4787; *Angew. Chem.* **2009**, *121*, 4879 – 4881.
[9] F. Wang, Z. Wang, L. Yin, R. Cheng, J. Wang, Y. Wen, T. A. Shifa, F. Wang, Y. Zhang, X. Zhan, J. He, *Chem. Soc. Rev.* **2018**, *47*, 6296 – 6341.
[10] L. Yang, K. Majumdar, H. Liu, Y. Du, H. Wu, M. Hatzistergos, P. Y. Hung, R. Tieckelmann, W. Tsai, C. Hobbs, P. D. Ye, *Nano Lett.* **2014**, *14*, 6275 – 6280.
[11] D. Hanlon, C. Backes, E. Doherty, C. S. Cucinotta, N. C. Berner, C. Boland, K. Lee, A. Harvey, P. Lynch, Z. Gholamvand, S. Zhang, K. Wang, G. Moynihan, A. Pokle, Q. M. Ramasse, N. McEvoy, W. J. Blau, J. Wang, G. Abellan, F. Hauke, A. Hirsch, S. Sanvito, D. D. O'Regan, G. S. Duesberg, V. Nicolosi, J. N. Coleman, *Nat. Commun.* **2015**, *6*, 8563.
[12] F. Wang, T. A. Shifa, P. Yu, P. He, Y. Liu, F. Wang, Z. Wang, X. Zhan, X. Lou, F. Xia, J. He, *Adv. Funct. Mater.* **2018**, *28*, 1802151.
[13] Z. Liu, N. Li, H. Zhao, Y. Du, *J. Mater. Chem. A* **2015**, *3*, 19706 – 19710.
[14] Y. Zhang, L. Yin, J. Chu, T. A. Shifa, J. Xia, F. Wang, Y. Wen, X. Zhan, Z. Wang, J. He, *Adv. Mater.* **2018**, *30*, 1803665.
[15] Z. Q. Zheng, J. D. Yao, B. Wang, Y. B. Yang, G. W. Yang, J. B. Li, *ACS Appl. Mater. Interfaces* **2017**, *9*, 43830 – 43837.
[16] R. Cheng, F. Wang, L. Yin, Z. Wang, Y. Wen, T. A. Shifa, J. He, *Nature Electronics* **2018**, *1*, 356 – 361.
[17] J. Zhou, Q. Zeng, D. Lv, L. Sun, L. Niu, W. Fu, F. Liu, Z. Shen, C. Jin, Z. Liu, *Nano Lett.* **2015**, *15*, 6400 – 6405.
[18] W. Ding, J. Zhu, Z. Wang, Y. Gao, D. Xiao, Y. Gu, Z. Zhang, W. Zhu, *Nat. Commun.* **2017**, *8*, 14956.
[19] T. Zhai, X. Fang, M. Liao, X. Xu, L. Li, B. Liu, Y. Koide, Y. Ma, J. Yao, Y. Bando, D. Golberg, *ACS Nano* **2010**, *4*, 1596 – 1602.
[20] W. Feng, W. Zheng, F. Gao, X. Chen, G. Liu, T. Hasan, W. W. Cao, P. Hu, *Chem. Mater.* **2016**, *28*, 4278 – 4283.
[21] M. S. Dresselhaus, G. Dresselhaus, *Adv. Phys.* **2002**, *51*, 1 – 186.
[22] A. Harvey, C. Backes, Z. Gholamvand, D. Hanlon, D. McAteer, H. C. Nerl, E. McGuire, A. Seral-Ascaso, Q. M. Ramasse, N. McEvoy, S. Winters, N. C. Berner, D. McCloskey, J. F. Donegan, G. S. Duesberg, V. Nicolosi, J. N. Coleman, *Chem. Mater.* **2015**, *27*, 3483 – 3493.
[23] Z. Sun, H. Xie, S. Tang, X. F. Yu, Z. Guo, J. Shao, H. Zhang, H. Huang, H. Wang, P. K. Chu, *Angew. Chem. Int. Ed.* **2015**, *54*, 11526 – 11530; *Angew. Chem.* **2015**, *127*, 11688 – 11692.
[24] V. Nicolosi, M. Chhowalla, M. G. Kanatzidis, M. S. Strano, J. N. Coleman, *Science* **2013**, *340*, 1226419.
[25] Z. Guo, H. Zhang, S. Lu, Z. Wang, S. Tang, J. Shao, Z. B. Sun, H. H. Xie, H. Y. Wang, X. F. Yu, P. K. Chu, *Adv. Funct. Mater.* **2015**, *25*, 6996 – 7002.
[26] J. Shao, H. Xie, H. Huang, Z. Li, Z. Sun, Y. Xu, Q. Xiao, X. F. Yu, Y. Zhao, H. Zhang, H. Wang, P. K. Chu, *Nat. Commun.* **2016**, *7*, 12967.
[27] J. Li, Z. Wang, Y. Wen, J. Chu, L. Yin, R. Cheng, L. Lei, P. He, C. Jiang, L. Feng, J. He, *Adv. Funct. Mater.* **2018**, *28*, 1706437.
[28] L. S. Lin, Z. X. Cong, J. B. Cao, K. M. Ke, Q. L. Peng, J. Gao, H. H. Yang, G. Liu, X. Chen, *ACS Nano* **2014**, *8*, 3876 – 3883.
[29] T. Liu, C. Wang, X. Gu, H. Guo, L. Cheng, X. Shi, L. Feng, B. Sun, Z. Liu, *Adv. Mater.* **2014**, *26*, 3433 – 3440.
[30] R. B. RJacobs-Gedrim, M. Shanmugam, N. Jain, C. A. Durcan, M. T. Murphy, T. M. Murray, R. J. Matyi, R. L. Moore, B. Yu, *ACS Nano* **2014**, *8*, 514 – 521.
[31] S. Marsillac, A. M. Combot-Marie, J. C. Bernede, A. Conan, *Thin Solid Films* **1996**, *288*, 14 – 20.
[32] J. Ye, S. Soeda, Y. Nakamura, O. Nittono, *Jpn. J. Appl. Phys.* **1998**, *37*, 4264 – 4271.
[33] Z. Zheng, J. Yao, J. Xiao, G. Yang, *ACS Appl. Mater. Interfaces* **2016**, *8*, 20200 – 20211.
[34] H. Peng, D. T. Schoen, S. Meister, X. Zhang, Y. Cui, *J. Am. Chem. Soc.* **2007**, *129*, 34 – 35.
[35] Y. Zhou, D. Wu, Y. Zhu, Y. Cho, Q. He, X. Yang, K. Herrera, Z. Chu, Y. Han, M. C. Downer, H. Peng, K. Lai, *Nano Lett.* **2017**, *17*, 5508 – 5513.
[36] G. W. Mudd, S. A. Svatek, T. Ren, A. Patane, O. Makarovsky, L. Eaves, P. H. Beton, Z. D. Kovalyuk, G. V. Lashkarev, Z. R. Kudrynskyi, A. I. Dmitriev, *Adv. Mater.* **2013**, *25*, 5714 – 5718.
[37] Y. Tan, X. Hu, M. Liu, X. Liu, X. Lv, Z. Li, J. Wang, Q. Yuan, *Chem. Eur. J.* **2017**, *23*, 10683 – 10689.
[38] F. Yang, Z. Yang, Y. Zhuo, Y. Chai, R. Yuan, *Biosens. Bioelectron.* **2015**, *66*, 356 – 362.
[39] J. Zhang, Y. Feng, J. Mi, Y. Shen, Z. Tu, L. Liu, *J. Hazard. Mater.* **2018**, *342*, 121 – 130.
[40] H. Wang, X. Yang, W. Shao, S. Chen, J. Xie, X. Zhang, J. Wang, Y. Xie, *J. Am. Chem. Soc.* **2015**, *137*, 11376 – 11382.
[41] H. Shen, J. Wang, H. Liu, Z. Li, F. Jiang, F. B. Wang, Q. Yuan, *ACS Appl. Mater. Interfaces* **2016**, *8*, 19371 – 19378.

Manuscript received: August 27, 2018
Revised manuscript received: September 28, 2018
Accepted manuscript online: October 3, 2018
Version of record online: November 21, 2018